American Journal of Applied Scientific Research
2025, Vol. 11, No. 3, pp. 152-159
https://doi.org/10.11648/j.ajasr.20251103.12

Research Article

Structural and Optical Properties of $SrAl_2O_4:Eu^{2+}$, Dy^{3+} Nanoparticles: Influence of Growth Temperature

Victor Saidi Kadenge[1, *], Sharon Kiprotich[2], Millien Kawira[1], Ali Halake Wako[1]

[1]Department of Physical Sciences, University of Embu, Embu, Kenya

[2]Department of Physical and Biological Sciences, Murang'a University of Technology, Murang'a, Kenya

Abstract

Persistent luminescent nanomaterials, such as $SrAl_2O_4:Eu^{2+}$, Dy^{3+}, have gained significant attention due to their ability to emit light after excitation, making them suitable for various optoelectronic and display applications. However, their thermal stability and luminescent efficiency are highly dependent on synthesis conditions. This study investigates the thermally stable properties of $SrAl_2O_4:Eu^{2+}$, Dy^{3+} nanoparticles (NPs) for the development of efficient luminous nanomaterials, focusing on how synthesis temperature influences their structural and optical characteristics. The NPs were synthesized at varying temperatures (500°C to 1000°C) and analyzed using X-ray diffraction (XRD), Fourier-transform infrared (FTIR) spectroscopy, UV-Vis spectroscopy, and scanning electron microscopy (SEM). Their luminescent properties under UV excitation were also evaluated. The NPs exhibited a monoclinic phase, with minor impurities at 500°C and 600°C. Higher synthesis temperatures shifted absorption edges to shorter wavelengths, with the band gap increasing up to 500°C but decreasing at 1000°C. SEM revealed irregular morphologies with pores and cracks, while crystal growth at elevated temperatures enhanced green emission, peaking at 700°C. Beyond 700°C, luminescence declined due to secondary phase formation and rare-earth ion oxidation. Due to their strong green emission and stability, these phosphors could be used in glow-in-the-dark signage, emergency exit indicators, and traffic signs, offering long-lasting visibility without external power sources. Optimized synthesis at 700°C ensures high performance, making them viable for commercial luminescent displays.

Keywords

Strontium Aluminate, Lattice Parameter, Crystallite Size, Band Gap, Phosphors

1. Introduction

Research on nanophase materials is receiving much attention because their size-dependent physical characteristics change significantly as particle sizes go closer to the nanometer scale [1]. The optical features and practical applications of nanoparticles have drawn the attention of humanity for an extended time. The optical properties possess a diverse array of practical uses across multiple disciplines, including but not limited to cathode rays, plasma display panels field emission displays, and safety signage [2]. These features of luminescent materials are contingent upon a multitude of factors, such as dimensions, morphology, and surface qualities, as well as additional variables like doping and interactions with the immediate surroundings or other nanostructure. Phosphors exhibit favorable characteristics when generated in

*Corresponding author: 1359@student.embuni.ac.ke (Victor Saidi Kadenge)

Received: 20 July 2025; **Accepted:** 30 July 2025; **Published:** 19 August 2025

the nanophase, rendering them a material of great potential. It is the grain size of luminescent materials that mostly affect their phosphorescent characteristics [1]. When the grain size is reduced to the nanoscale, a variety of novel behaviors can be achieved. Various strategies have been utilized to produce nanophase phosphors, such as the solid-state method, solution combustion method, and co-precipitation [3]. Regarding most NPs, the time frame of light emissions decay generally is less than mere milliseconds following the removal of excitation.

while maintaining structural stability.

Despite extensive research on extending the afterglow duration of luminescent nanomaterials, a critical gap remains: the lack of a well-defined optimum synthesis temperature that maximizes luminescence [4]. Previous studies have explored various synthesis methods (e.g., solid-state, combustion, co-precipitation) but the temperature-dependent luminescence behavior of $SrAl_2O_4$:Eu^{2+}, Dy^{3+} NPs has not been systematically optimized [5, 6]. Many studies report enhanced afterglow at different temperatures, but no consensus exists on the ideal synthesis conditions that balance crystallinity, phase purity, and luminescent intensity. Some works suggest high temperatures improve crystallinity, while others indicate that excessive heat leads to secondary phase formation and rare-earth ion oxidation, degrading performance [7]. Alkaline earth aluminate materials have recently gained considerable attention. One material that has garnered significant attention in academic research is SrAl2O4. This material has been extensively explored owing to its inherent characteristics such as structural stability, chemical resistance, minimal toxicity, and [6] exceptional optical qualities. Due to its broad band gap, $SrAl_2O_4$ exhibits a lack of absorption across the whole visible spectrum. This property essentially prevents the reabsorption of light produced by rare earth (RE) ions. Doping is a useful and inexpensive way to modify the structural and optical properties of SrAl2O4. These phenomena are fascinating because they do not involve the use of radioactive isotopes. In contrast to conventional sulphide phosphors, aluminate has several favorable properties, including increased radiation intensity, improved color purity, extended afterglow, chemical stability, safety and non-radioactive properties [8]. The study of aluminates and related structures has attracted much attention due to their potential in occupational safety [9]. A phosphor substance often recognized in the field is zinc sulfide (ZnS), which has limited longevity [10]. To solve this problem, researchers have found that alkaline earth aluminates are a viable alternative [11]. These materials are chemically stable and have long-lasting luminescent properties. Therefore, they are widely used as matrix materials in modern luminescent devices, which provide better luminescent performance [11, 12]. Luminescence can occur in the wavelength range of the electromagnetic spectrum, extending from ultraviolet to red. The intensity and characteristics of this luminescence are strongly influenced by the specific characteristics of the host lattice [13]. RE-AL_2O_4-based phosphor aluminates exhibit photoluminescence characterized by a longer luminescence emission [14]. Many methods have been discovered to synthesize phosphorous materials belonging to the alkaline-earth aluminate family [15]. Some phosphors with particularly impressive luminescent properties are the blue-emitting calcium aluminates doped with europium and co-doped with neodymium. $CaAl_2O_4$: Eu^{2+}, Nd^{3+}, the strontium aluminates $SrAl_2O_4$ which produce a green light when activated with Eu^{2+} and co-activate with Dy^{3+} phosphor, and the yellow-emitting $BaAl_2O_4$: Eu^{2+}, Dy^{3+} phosphor [16]. The luminous property of strontium aluminate is enhanced through the incorporation of Dy^{3+} ions into the matrix, achieved by creating highly concentrated trapping levels. The strontium aluminate activated with Europium ions and co-doped Dysprosium is a crucial material in terms of its long-afterglow characteristics [17]. One often employed method for enhancing the characteristics of these materials is the introduction of appropriate cations into the parent lattice [18]. The aforementioned qualities are also influenced significantly by the method employed for synthesis and the synthesis temperature.

This paper presents a comprehensive investigation of the synthesis of strontium aluminate using the solution combustion technique [19]. Temperature is a crucial factor in thermodynamics that significantly influences the morphology, crystallite size, and surface characteristics of the nanoparticles being synthesized [20]. This investigation was conducted to examine the impact of this variable on both the optical and structural properties of strontium aluminate doped $Eu^{2+}$with and co-doped Dy^{3+}. The investigation is conducted using X-ray diffractometer (XRD) and other optical characterization methods. The aluminates under study follows a general formula $Sr_{0.97}Al_2O_4$: $Eu^{2+}_{0.01}Dy^{3+}_{0.02}$. The ionic radii of Eu_{2+} and Dy^{3+} are reported to be 1.09Å and 0.908Å, respectively. In regards to the information provided, it is anticipated that these ions have the potential to substitute Sr, which exhibits a radius of the ions of around 1.12Å and does not induce significant structural deformation.

In this study, we propose a simple approach to create nanostructured powders of $SrAl_2O_4$:Eu^{2+}, Dy^{3+} at various furnace temperatures utilizing the combustion process. The combustion method shows potential as a viable method for producing various nanopowders. The technique is very adaptable, efficient, and operates at (600 ℃) [23]. It enables uniform doping in a single step and does not call for a reducing atmosphere for powder preparation. The particles produced using conventional combustion methods have dimensions inside the nanometer scale. The element strontium aluminate hosts are appealing as a result of their exceptional phosphorescent characteristics and high longevity. Functional inorganic materials find extensive use in various applications such as persistent luminous paints, inks, and ceramics [21, 22].

2. Experimental Procedure

2.1. Synthesis of $SrAl_2O_4$: Eu^{2+}, Dy^{3+} Phosphors

The synthesis of strontium aluminate doped with Eu2+ and co-doped with Dy^{3+} involved the utilization of high-purity start-

ing materials, including $Sr(NO_3)_2$ (99.90%), $Al(NO_3)_3 \cdot 9H_2O$ (98.99%), $Eu(NO_3)_3 \cdot 6H_2O$ (99%), $Dy(NO_3)_3 \cdot 5H_2O$ (98%), $CO(NH_2)_2$ (99.99%) along with a H_3BO_3 (99.90%) were supplied by sigma Aldrich. The synthesis method was adapted from the literature [23]. A set of six samples of strontium aluminate phosphor doped with Eu^{2+} and co-doped Dy^{3+} phosphor were prepared using the solution combustion approach. Solutions were prepared by dissolving the stoichiometric amount of the precursors, dopants, 20-fold molar excess urea as fuel and along with a trace amount of boric acid as reducer in 10 ml of deionized water. All mixtures were then stirred for 30 minutes on a magnetic stirrer. After that, six silica crucibles were filled with the mixture. After being transferred to a larger crucible, the solutions were placed in a muffle furnace. The furnace was maintained at temperatures of 500 ℃, 600 ℃, 700 ℃, 800 ℃, 900 ℃, and 1000 ℃ for samples 1, 2, 3, 4, 5, and 6 respectively, one at a time. The process commenced with the dehydration of the solution through boiling, which was then followed by the release of gases (such as carbon oxides, nitrogen, and ammonia) as a result of significant decomposition. Subsequently, the reagent underwent spontaneous ignition, leading to combustion and generating a substantial quantity of frothy and copious ash. The combination underwent a process of frothing and swelling, resulting in the formation of foam. This foam then decomposed with a flame. The process continued for a short time, after which the crucible was removed from the furnace and then placed in an open environment to facilitate cooling in the free atmosphere. After cooling process, the material acquired a fluffy texture. Afterward, the phosphor was finely powdered using an agate pestle and mortar.

2.2. Characterizations

The crystalline composition and phase development of the polycrystalline strontium aluminate were analyzed using XRD. This analysis was conducted using a Rigaku Miniflex XRD, with CuKα (0.15406 nm) radiation, spanning the angle range of 2θ (10 °-90 °) operating at 40kV and 4mA. The sample diffractogram was analyzed using the VESTA software for phase identification. Fourier transform infra-red spectrometer (FTIR) equipment was utilized to examine the area encompassing fingerprints (400-1400 cm^{-1}) and the area associated with the functional group (1400-4000 cm^{-1}). An ultra-violet visible spectrophotometer (UV-Vis) Perkin Elmer, Lambda 950 was used to investigate the material's optical energy band gap.

3. Results and Discussion

3.1. Morphology and Structure

XRD is a distinctive method used to ascertain the crystal structure and crystallinity of a material. The XRD profiles of the synthesized $SrAl_2O_4$:Eu^{2+}, Dy^{3+}phosphor are presented in Figure 1.

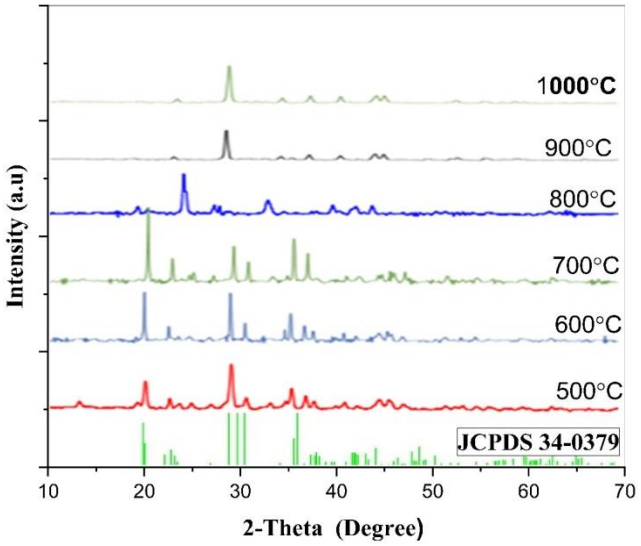

Figure 1. *XRD patterns of SAED prepared at different furnace temperatures.*

Five prominent XRD peaks at 2θ values of 19.96, 28.46, 29.27, 29.98, and 35.11 degrees correspond to the crystallographic planes (0 1 1), (-2 1 1), (2 2 0), (2 1 1), and (0 3 1), respectively. These XRD peaks of the $SrAl_2O_4$ crystal lattice configuration matched well with the standard JCPDS file No. 34-0379. The synthesized samples exhibited broader and more peaks, which suggest a smaller particle size and an increase in the level of crystallinity [3]. $SrAl_2O_4$:Eu^{2+}, Dy^{3+} exhibited two distinct phases, namely a hexagonal phase (referred to as the β-phase) at high [21] temperatures and a monoclinic phase (referred to as the α-phase) at low temperatures [24]. The XRD profiles found confirm the presence of a dominating monoclinic $SrAl_2O_4$:Eu^{2+}, Dy^{3+}phase. The crystal structure of the produced powders were determined to be in the low-temperature monoclinic phase with a space group P_{21} using VESTA software. The nanoparticle crystallite size were determined by calculating the full width at half maximum (FWHM) values using (220) employing the Debye-Scherer formula. The as-prepared $SrAl_2O_4$:Eu^{2+}, Dy^{3+} samples exhibited crystallite sizes ranging from 35 to 42 nm. The crystallite size calculated using Scherrer's formula [25] represented in equation (1).

$$D = \frac{\kappa \lambda}{\beta cos\theta} \quad (1)$$

where K denotes a fixed value that varies depending on the form of the grain, λ represents the wavelength of X-rays employed, β corresponds to FWHM and θ is the Bragg angle were 40.86, 36.85, 35.74, 38.81, 39.02, 41.62 nm synthesized at 500 ℃, 600 ℃, 700 ℃, 800 ℃, 900 ℃, and 1000 ℃. Consequently, it was observed that the particle size exhibited a significant correlation with the synthesis temperature. Enlargement in crystallite size suggests that tiny particles are diffusing and combining to produce bigger particles as the synthesis temperature increases [20]. Furthermore, arise in the

$SrAl_2O_4:Eu^{2+}$, Dy^{3+} crystallite size upon raising the synthesis temperature supports the idea that a small crystallite size is necessary to enable the formation of a monoclinic steady crystalline structure [11]. The lattice parameters for monoclinic and hexagonal phases did not match well with standard bulk indicating that the material is under strain(ε)[25]. The strain computation provides more details regarding the structural features of $SrAl_2O_4:Eu^{2+}$, Dy^{3+} which can be determined by applying equation (2)

$$\varepsilon = \frac{\beta}{4tan\theta} \quad (2)$$

The strain of the synthesized nanocrystalline particles was observed to rise from 0.280 to 0.320 as the synthesis temperature is raised to 700 ℃. However, an additional rise in the furnace temperature causes the strain to fall to 0.243. This rise in strain is attributed to the rise in dislocation density in the $SrAl_2O_4:Eu^{2+}$, Dy^{3+}. The degree of dislocation (δ) is expressed to be the length of the dislocations per unit volume. The determination of dislocation lines per unit volume is accomplished through the utilization of the formula. The expression (3)

$$\delta = \frac{1}{D^2} \quad (3)$$

Table 1 presents δ and ε values for various nanostructure strontium aluminates phosphors. A notable observation is that when the value of ε increases, there is a decrease in the crystallite size D, accompanied by an increase in the δ values. The reduction in δ and ε serves as an indication that phosphors are undergoing a transition toward a more crystalline state [23].

Table 1. *The calculated values of the structural parameters of as-prepared $SrAl_2O_4:Eu^{2+}$, Dy^{3+} at different growth temperatures.*

Sample	Lattice parameters, *a* (nm)	Strain (ε)	Dislocation density (δ)	Crystallite size nm (D)
S_1	0.844	0.280	5.99×10^{-4}	40.86
S_2	0.825	0.311	7.36×10^{-4}	36.85
S_3	0.831	0.320	7.82×10^{-4}	35.74
S_4	0.828	0.260	6.64×10^{-4}	38.81
S_5	0.834	0.258	6.57×10^{-4}	39.02
S_6	0.829	0.243	5.77×10^{-4}	41.62

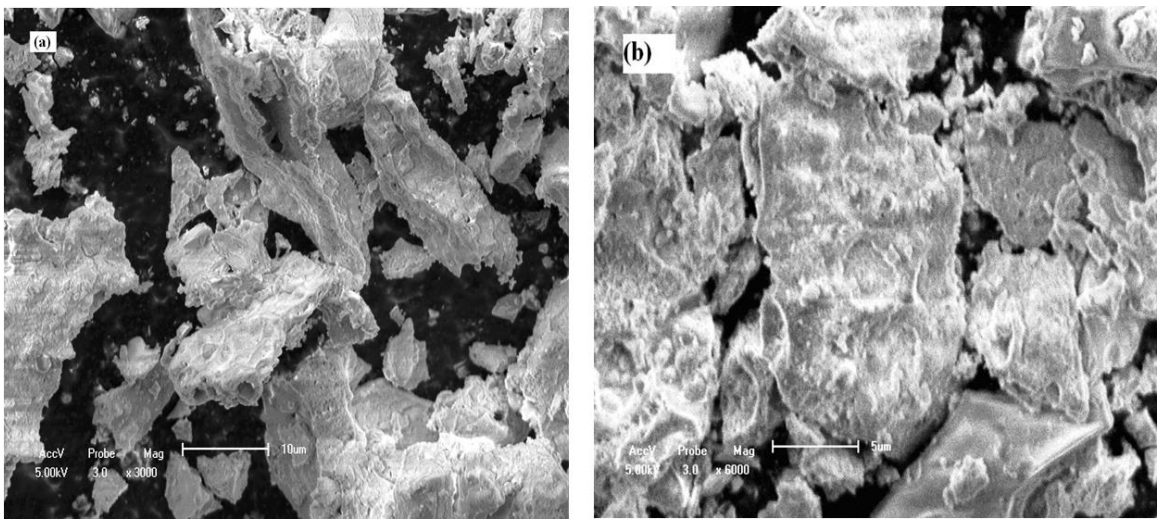

Figure 2. *The SEM images of the synthesized $SrAl_2O_4:Eu^{2+}$, Dy^{3+} nanomaterial (a) synthesized at $600°C$, (b) synthesized at $700°C$.*

The SEM analysis was conducted to examine the surface appearance and crystallite size of the synthesized phosphor powders. Figure 2 presents the SEM micrographs of $SrAl_2O_4:Eu^{2+}$, Dy^{3+} synthesized at 600 ℃ (a) and at 700 ℃ (b). The images indicate that the majority of the particles exhibit a nearly spherical shape with an evenly sized distribution. A detailed inspection of these images provides a distinct particle-like morphology, characterized by a predominance of

spherical particles, with a standard particle size ranging from 35 to 42 nm. Additionally, there are significant voids and pores on the surface, attributed to gas release throughout the synthesis process.

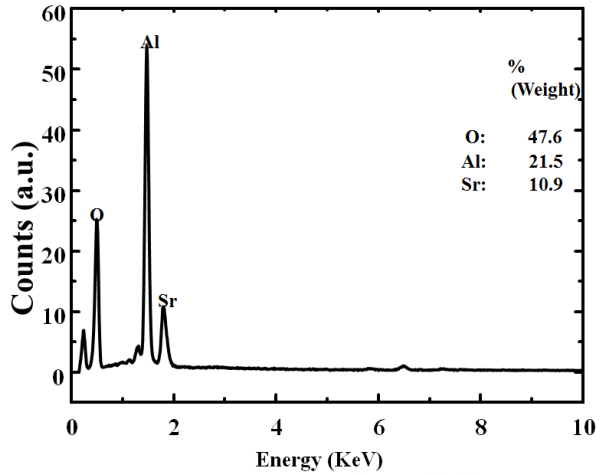

Figure 3. *Point EDS results of the $SrAl_2O_4:Eu^{2+}$, Dy^{3+} synthesized at 700°C.*

The findings of the elemental analysis using EDS are presented in Fig. 3, which illustrates the existence of the anticipated elements, namely oxygen, aluminum, and strontium, in percentages consistent with the originally calculated amounts [26]. The majority of the components used in the phosphor nanoparticles are depicted in Figure 3. Eu^{2+} and Dy^{3+} were undetectable by EDS due to their minimal levels.

3.2. U.V. Visible

The band-gap value of various $SrAl_2O_4:Eu^{2+}$, Dy^{3+} phosphor samples were determined by recording their absorption bands in the spectrum range of 200 to 800 nm.

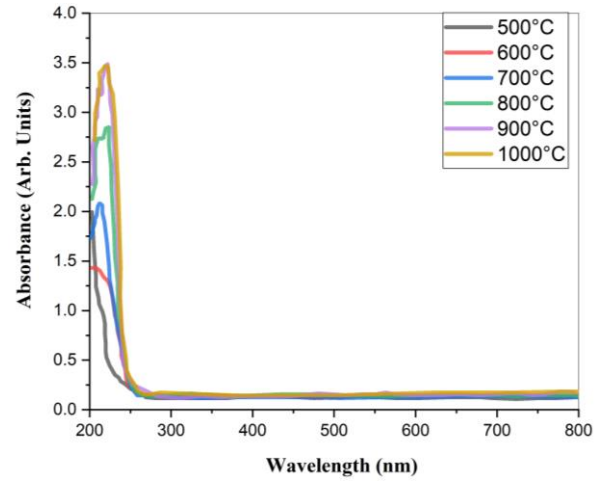

Figure 4. *Graph showing absorbance spectra of $SrAl_2O_4:Eu^{2+}$, Dy^{3+}(SAED) synthesized at different combustion temperatures.*

The band gaps of nanocrystalline particles would be altered by quantum entanglement impacts, which are dependent on the size of the nanoparticles [16]. Consequently, this might impact the absorption wavelength of the generated materials. Figure 2 demonstrates a strong relationship between the growth temperature and the movement of absorbance peaks towards longer wavelengths [12]. An increase in furnace temperature resulted in a shift of the absorption edges towards greater wavelengths [13]. The estimated absorption edges were 240, 249, 250, 251, 255, and 260 nm for growth temperatures of 500, 600, 700, 800, 900 and 1000 ℃ respectively. The Stokes shift of $SrAl_2O_4:Eu^{2+}$, Dy^{3+} nanoparticles were greater when the powders are produced in open air, mostly because of the intense phonon coupling [5, 6, 8, 9]. The noted Stoke shift was a result of the band-edge transition, which was influenced by the variation of crystal sizes. The observed correlation between the Stoke shift and synthesis temperature can be explained by the accelerated nucleation process at greater temperatures [13]. As a result, particles with a larger area of contact are formed, which facilitates a greater number of interactions between electrons and holes [26].

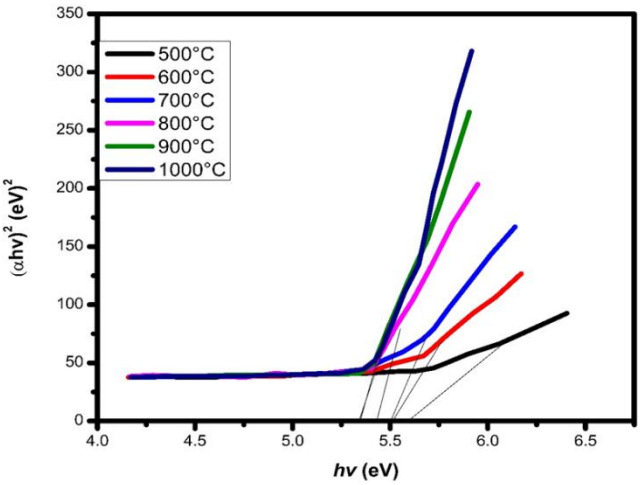

Figure 5. *Tauc plot ($(ahv)^2$ vs hv) to determine the band gap energy of the$SrAl_2O_4:Eu^{2+}$, Dy^{3+} phosphors.*

The absorbance spectra and the Tauc relation, which is frequently used to determine the near band-edge optical absorption of semiconductors, were utilized to estimate the energy band gap of SAED. The band gap energy of the as-prepared SAED can be estimated by extrapolating the linear component *hv* and identifying the point where it intersects. The $SrAl_2O_4:Eu^{2+}$, Dy^{3+} compound exhibited band gap values of 5.62, 5.51, 5.50, 5.49, 5.44, and 5.4 eV at furnace temperatures of 500, 600, 700, 800, 900 and 1000 ℃, respectively. Figure 3 displays the band gap value of the SAED NPs in their original state. The measured results exhibit a modest elevation compared to the documented bulk estimation of 4.47 eV [27]. The increase in optical band gap is ascribed to the extremely small dimensions of the crystallite size and the

resulting entrapment of electronic energy in the NPs [27]. Overall NPs samples generated in the present research had a crystallite size of approximately 41 nm, as determined by XRD tests. The following explains the significantly larger optical band gaps found compared to the bulk value.

Deriving a precise value for E_g from the experimental curve is challenging in practice, mostly due to the influence of temperature and the potential presence of excitonic characteristics toward the lower end of the conduction band. The absence of distinct features in the spectrum poses challenges in determining a precise value for E_g. Conclusively, the materials used in this work have a wide band-gap characteristic.

3.3. Fourier Transform Infrared (FTIR) Spectroscopy

FTIR is a rapid and accurate method for qualitatively measuring compounds. The FTIR examination is a crucial instrument for enhancing comprehension of the qualities of the acquired sample. The central infrared range (4000-400 cm^{-1}) [27] is precious for organic and inorganic substances spectroscopic analysis. Figure 4 displays the FTIR transmittance profile of the strontium aluminate NPs. The infrared spectra of strontium aluminate show distinct prominent band at 3399 cm^{-1} and weaker bands at approximately 1800-1700 cm^{-1} [27] associated with vibrations caused by the stretching and bending vibrations of O-H [27]. A high level of dampness in the surroundings may result in the O-H [27] group formation in$SrAl_2O_4:Eu^{2+}$, Dy^{3+}. The infrared profile spectra of $SrAl_2O_4:Eu^{2+}$, Dy^{3+}phosphors exhibit a prominent peak at a wavenumber of 1482.23 cm^{-1} [27].

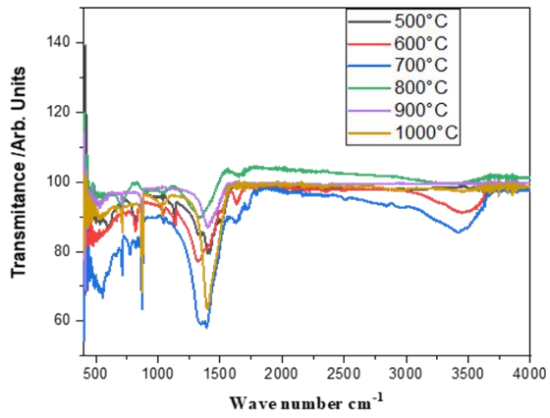

Figure 6. *FT-IR spectra of $SrAl_2O_4:Eu^{2+}$, Dy^{3+}prepared at different furnace temperatures.*

The precise provenance of this summit, however, remains somewhat ambiguous. The peaks detected at this specific wavenumber cannot be ascribed to the $Sr(NO_3)_2$ compounds synthesized as precursors during fabrication. These results align with the results published by Lu et al [24]. The peak at 1500-1600 cm^{-1} [28] indicates the stretching mode of the C = O [27, 28] bond in a carbonyl functional group on the crystal surface. Table 2 shows summary of results obtained from FT-IR analysis.

Table 2. *Table summarizing the FTI-IR absorption peaks for $SrAl_2O_4:Eu^{2+}$, Dy^{3+} phosphors.*

Absorption peaks	Assignment
3750	N-H stretching vibrations
3500	O-H stretching vibrations
1712	C=O stretching vibrations
1360	N-O stretching vibrations
742	Sr-O stretching vibrations
437	O-Al-0stretching vibrations

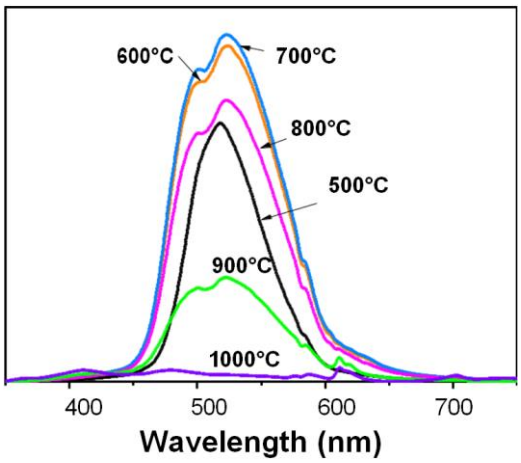

Figure 7. *PL spectra of SrAl2O4-based phosphor powders synthesis at various temperatures.*

Figure 7. illustrates the photoluminescence spectra of phosphor powders at an excitation wavelength of 345 nm. The photoluminescence spectrum of 700 ℃ powders exhibited a peak at 520 nm, corresponding to the green light emission band. The luminescence can be attributed to the characteristic $4f^65d^1$-$4f^7$ transition of the Eu^{2+} ion in $SrAl_2O_4$. The spectrum form exhibited modest asymmetry due to the emission of fluorescent pigment included in the phosphor. For such specimens, photoluminescence intensity significantly increased at elevated growth temperatures, peaking at approximately 700 ℃. An additional rise in growth temperatures resulted in diminished luminous intensity due to phase change and the oxidation of the Eu^{2+} ion. Furthermore, two emission peaks at 500 nm and 524 nm were noted. This may be elucidated by a modification in the oxidized Eu^{2+} milieu. Prior studies have indicated that the permitted 4f-5d transitions are significantly affected by the chemical environment of the Eu^{2+} ion, leading to a variation in the emission of the Eu^{2+} ion from

ultraviolet to red in aluminates. The emission of Eu^{2+} is observed to move to greater wavelengths when the synthesis temperature increase.

Conclusion

The $SrAl_2O_4:Eu^{2+}$, Dy^{3+} NPs were effectively synthesized using a solution combustion method at different temperatures. The XRD experiments demonstrated the presence of nanocrystalline nanoparticles in a monoclinic and hexagonal phase. Average crystallites sizes of the as-prepared $SrAl_2O_4:Eu^{2+}$, Dy^{3+} NPs, determined using the Debye-Scherrer equation, exhibited an upward trend as the synthesis temperature increased 40.86, 36.85, 35.81, and 39.02, 41.62 nm prepared at 500, 600, 800, 900, and 1000 ℃, respectively. The UV-Vis examination revealed the temperature-dependent characteristics of the synthesized $SrAl_2O_4:Eu^{2+}$, Dy^{3+} sample. The absorption edges exhibited a red shift with increasing synthesis temperature. The calculated optical band gap showed an inverse relationship with the furnace temperature. Increasing the synthesis temperature led to a decrease in the optical band gap, which can be ascribed to growth in the crystallite size. The synthesis temperature is crucial in producing $SrAl_2O_4:Eu^{2+}$, Dy^{3+} nanoparticles with adjustable material characteristics. The $SrAl_2O_4:Eu^{2+}$, Dy^{3+} nanoparticles, synthesized at a temperature of 700 ℃ using the aqueous method, exhibited favorable characteristics suitable for creating a luminous sign for occupational safety purposes.

Abbreviations

JCPDS	Joint Committee on Powder Diffraction Standards
NPS	Nanoparticles
SAED	Strontium Aluminate, Europium and Dysprosium
SEM	Scanning Electron Microscope
RE	Rare Earth

Acknowledgments

The authors thank Murang'a University of Technology, Pwani University, and Meneng'ai Geothermal Power Plant for their help in performing characterization of the prepared samples at their centers.

Author Contributions

Victor Saidi Kadenge: Conceptualization, Formal Analysis, Validation, Writing - original draft, Writing - review & editing

Sharon Kiprotich: Investigation, Methodology, Supervision

Millien Kawira: Investigation, Methodology, Resources, Supervision

Ali Halake Wako: Investigation, Methodology, Resources, Supervision

Data Availability Statement

The information supporting the results of the present research can be acquired from the author(s) upon reasonable request.

Conflicts of Interest

The authors declare no conflicts of interest.

References

[1] S. A. M. Issa et al., "Fabrication of newly developed tungsten III-oxide glass family: Physical, structural, mechanical, radiation shielding effectiveness," Optik (Stuttg), vol. 259, p. 169025, Jun. 2022, https://doi.org/10.1016/J.IJLEO.2022.169025

[2] J. Bierwagen et al., "Probing traps in the persistent phosphor SrAl2O4:Eu2+, Dy3+, B3+ - A wavelength, temperature and sample dependent thermoluminescence investigation," J Lumin, vol. 222, p. 117113, Jun. 2020, https://doi.org/10.1016/J.JLUMIN.2020.117113

[3] X. Hu, L. Wu, H. Yin, G. Li, and D. Guo, "Effects of co-activator species and transition metal ions doping on structure and fluorescence properties of strontium aluminate phosphors," Journal of Materials Science: Materials in Electronics, vol. 30, no. 4, pp. 3804-3810, Feb. 2019, https://doi.org/10.1007/s10854-019-00664-y

[4] D. Kim, H. E. Kim, and C. H. Kim, "Effect of composition and impurities on the phosphorescence of Green-Emitting alkaline earth aluminate phosphor," PLoS One, vol. 11, no. 1, Jan. 2016, https://doi.org/10.1371/journal.pone.0145434

[5] Z. Ni et al., "Effect of the Concentration of SrAl2O4: Eu2+and Dy3+(SAO) on Characteristics and Properties of Environment-Friendly Long-Persistent Luminescence Composites from Polylactic Acid and SAO," Scanning, vol. 2021, 2021, https://doi.org/10.1155/2021/6337768

[6] T. Peng, H. Yang, X. Pu, B. Hu, Z. Jiang, and C. Yan, "Combustion synthesis and photoluminescence of SrAl2O4: Eu, Dy phosphor nanoparticles," Mater Lett, vol. 58, no. 3-4, pp. 352-356, Jan. 2004, https://doi.org/10.1016/S0167-577X(03)00499-3

[7] F. Ayachi, K. Saidi, and M. Dammak, "Exploring luminescence quenching mechanisms and temperature sensing capabilities of LiSrYW3O12:Sm3+ phosphors," Mater Adv, vol. 5, no. 15, pp. 6162-6169, Jul. 2024, https://doi.org/10.1039/D4MA00276H

[8] B. Yuan et al., "Effect of soil elements (Si, Al, and Ca) on the performance and structure of simulated An3+ radioactive contaminated soil by microwave sintering," J Environ Chem Eng, vol. 11, no. 3, p. 109751, Jun. 2023, https://doi.org/10.1016/J.JECE.2023.109751

[9] R. Snellings, P. Suraneni, and J. Skibsted, "Future and emerging supplementary cementitious materials," Cem Concr Res, vol. 171, p. 107199, Sep. 2023, https://doi.org/10.1016/J.CEMCONRES.2023.107199

[10] X. Hao, H. Sun, Z. Ren, Z. Huang, Y. Xu, and J. Li, "Recent advances in zinc sulfide-based anode regulation strategy for Na-ion batteries," J Energy Storage, vol. 97, p. 112847, Sep. 2024, https://doi.org/10.1016/J.EST.2024.112847

[11] S. K. Mohapatra, H. S. Maharana, S. Khan, S. Das, and K. Annapurna, "Novel Eu3+ doped mixed alkaline-earth zinc silico-aluminate glass for white-light-emitting diode, finger-print, and security ink application," Opt Mater (Amst), vol. 149, p. 115051, Mar. 2024, https://doi.org/10.1016/J.OPTMAT.2024.115051

[12] W. Lv, Y. Song, and Z. Mo, "Synthesis of metal-organic framework-luminescent guest (MOF@LG) composites and their applications in environmental health sensing: A mini review," Talanta, vol. 283, p. 127105, Feb. 2025, https://doi.org/10.1016/J.TALANTA.2024.127105

[13] D. Wei, Y. Teng, X. Yang, Y. Liu, and B. Ram Lee, "Luminescence spectra and site-occupation of Eu3+ centres in lithium antimonate LiSbO3 lattice," Microchemical Journal, vol. 204, p. 111150, Sep. 2024, https://doi.org/10.1016/J.MICROC.2024.111150

[14] L. Dong, S. Yang, C. Yang, B. Shao, J. Hou, and Y. Fang, "Multiple lattice sites driven broadband yellow emitting Ca8-y-zSryBazMgLa (PO4)7: Eu2+ solid solution phosphor with improved luminescence for high-quality white LED," Ceram Int, Apr. 2025, https://doi.org/10.1016/J.CERAMINT.2025.04.091

[15] R. C. Ropp, "Group 13 (B, Al, Ga, In and Tl) Alkaline Earth Compounds," Encyclopedia of the Alkaline Earth Compounds, pp. 481-635, Jan. 2013, https://doi.org/10.1016/B978-0-444-59550-8.00006-5

[16] M. Malkamäki et al., "Persistent luminescence excitation spectroscopy of BaAl2O4:Eu2+, Dy3+," Physica B Condens Matter, vol. 593, p. 411947, Sep. 2020, https://doi.org/10.1016/J.PHYSB.2019.411947

[17] H. S. Roh et al., "Enhanced photoluminescence property of Dy3+ co-doped BaAl2O4:Eu2+ green phosphors," Ceram Int, vol. 38, no. 1, pp. 443-447, Jan. 2012, https://doi.org/10.1016/J.CERAMINT.2011.07.025

[18] J. LI, J. WANG, Y. YU, Y. ZHU, and M. GE, "Preparation and luminescence properties of rare-earth doped fiber with spectral blue-shift: SrAl2O4:Eu2+, Dy3+ phosphors/triarylsulfonium hexafluoroantimonate based on polypropylene substrate," Journal of Rare Earths, vol. 35, no. 6, pp. 530-535, Jun. 2017, https://doi.org/10.1016/S1002-0721(17)60944-X

[19] A. Yegane, H. Khalili, and Z. Talebi, "Synthesis of engineered silica aerogel containing SrAl2O4: Eu2+, Dy3+ to improve luminescence efficiency, thermal and water stability and optical properties," J Non Cryst Solids, vol. 585, p. 121521, Jun. 2022, https://doi.org/10.1016/J.JNONCRYSOL.2022.121521

[20] S. Liu, Y. Cui, X. Sun, Z. Jiao, K. An, and Y. Wu, "Transparent SrAl2O4:Eu2+, Dy3+ glass-ceramics with significant mechanoluminescence," J Eur Ceram Soc, vol. 44, no. 13, pp. 7921-7926, Oct. 2024, https://doi.org/10.1016/J.JEURCERAMSOC.2024.05.045

[21] S. Ye et al., "The enhancing luminescence of B2O3-doped SrAl2O4: Eu2+, Dy3+ single crystals," J Lumin, vol. 277, p. 120920, Jan. 2025, https://doi.org/10.1016/J.JLUMIN.2024.120920

[22] H. Xue, M. Yang, J. Sun, and C. Zhang, "Study on the flux for SrAl2O4: Eu2+, Dy3+ phosphor preparation used in fluorescent fiber," Ceram Int, vol. 50, no. 1, pp. 1137-1146, Jan. 2024, https://doi.org/10.1016/J.CERAMINT.2023.10.206

[23] S. Kiprotich, M. O. Onani, and F. B. Dejene, "High luminescent L-cysteine capped CdTe quantum dots prepared at different reaction times," Physica B Condens Matter, vol. 535, pp. 202-210, Apr. 2018, https://doi.org/10.1016/J.PHYSB.2017.07.037

[24] L. A. Lumper-Wimler et al., "Phase transformations and metastable states in a Cu-20 m.% Sn alloy: An integrated HEXRD, TEM, and APT investigation," J Alloys Compd, vol. 1026, p. 180399, May 2025, https://doi.org/10.1016/J.JALLCOM.2025.180399

[25] D. S. Kshatri and A. Khare, "Comparative study of optical and structural properties of micro- and nanocrystalline SrAl2O4: Eu2+, Dy3+ phosphors," J Lumin, vol. 155, pp. 257-268, Nov. 2014, https://doi.org/10.1016/J.JLUMIN.2014.06.028

[26] B. P. Zhu et al., "Structure and Electrical Properties of (111)-Oriented Pb(Mg1/3Nb2/3)O3—PbZrO3—PbTiO3 Thin Film for Ultra-High-Frequency Transducer Applications," IEEE Trans Ultrason Ferroelectr Freq Control, vol. 58, no. 9, pp. 1962-1967, 2011, https://doi.org/10.1109/TUFFC.2011.2038

[27] Z. Xue, S. Deng, Y. Liu, B. Lei, Y. Xiao, and M. Zheng, "Synthesis and luminescence properties of SrAl2O4:Eu2+, Dy3+ hollow microspheres via a solvothermal co-precipitation method," Journal of Rare Earths, vol. 31, no. 3, pp. 241-246, Mar. 2013, https://doi.org/10.1016/S1002-0721(12)60265-8

[28] Y. YU et al., "Structural characterization and optical properties of long-lasting CaAl2O4:Eu2+, Nd3+ phosphors synthesized by microwave-assisted chemical co-precipitation," Journal of Rare Earths, vol. 35, no. 7, pp. 652-657, Jul. 2017, https://doi.org/10.1016/S1002-0721(17)60959-1